A&A 382, 746–751 (2002)
DOI: 10.1051/0004-6361:20011635

Astronomy & Astrophysics

Co-phasing of segmented telescopes: A new approach to piston measurements

I. Optical concept

V. V. Voitsekhovich[1], S. Bara[2], and V. G. Orlov[1]

[1] Instituto de Astronomia, UNAM AP 70-264 Cd. Universitaria, 04510 Mexico DF, Mexico
[2] Area de Optica, Departamento de Fisica Aplicada, Facultade de Fisica, Universidade de Santiago de Compostela, Campus Sur, 15706 Santiago de Compostela, Galicia, Spain
e-mail: fagosxbv@usc.es

Received 23 July 2001 / Accepted 2 October 2001

Abstract. One of the main problems arising in the co-phasing of segmented telescopes is the problem of measurements of the relative pistons among the segments. These measurements become especially complicated when the pistons are in order of wavelength fractions. In this paper we present a new approach relative piston measurements which allows for a high-accuracy reconstruction of small pistons. Our approach is based on the shearing interferometry and compared to existed methods it has the following advantages: a high accuracy of piston reconstruction in presence of high levels of noise is combined with the ability to retrieve the pistons taking into account the segment's aberrations.

Key words. instrumentation: miscellaneous – techniques: miscellaneous

1. Introduction

Presently there are two concepts in telescope construction: telescope with monolithic primary mirrors and telescope with segmented primary mirrors. As it is widely recognized by the scientific community, a primary segmented mirror is preferable for big telescopes (usually if it is bigger than 8 m). This preference is dictated by two main reasons. The first reason is a technological one: either it is not possible to fabricate a monolithic mirror of the required size, or it is impossible to provide the desired mirror quality, or the cost of mirror fabrication is too high. The second reason is related to mirror transportation: if a mirror is going to be big enough, it is often ether impossible to transport it to the telescope site, or it requires to build new, very expensive and quite special transportation facilities.

Compared to monolitic mirrors, however, there is one specific problem associated with segmented ones: the problem of mirror co-phasing. Because most future big telescopes are expected to have segmented mirrors, the co-phasing problem is a real one, and it attracts growing attention of researchers. The main difficulty arising in the co-phasing problem is the measurement of relative pistons among the segments. While the technique of big piston measurements (the broad-band co-phasing) is practically developed (Chanan et al. 1998), there are still certain problems related to the small piston reconstruction (the narrow-band co-phasing) when the piston $|\Delta| < \lambda/4$. Presently two main methods of small piston measurements based on the Shack-Hartmann test (Chanan et al. 2000) and curvature sensing (Rodriguez-Ramos et al. 1997; Chanan et al. 1999; Rodriguez-Ramos et al. 2000; Cuevas et al. 2000; Orlov et al. 2000) have been developed. These methods attempt to reconstruct the relative piston by measuring the phase discontinuity near to the segment's border. While the piston is big compared to segment's aberrations, the border measurements provide adequate information for the co-phasing. However, as soon as the piston becomes compared to the segment's aberrations, one has to measure the difference between the pistons averaged over the corresponding segments. Also, due to technological reasons, real segments may have quite big manufacturing border defects. Because these defects are located inside relatively small areas, they affect only slightly the overall image quality. However, they can

Send offprint requests to: V. V. Voitsekhovich,
e-mail: voisteko@astroscu.unam.mx

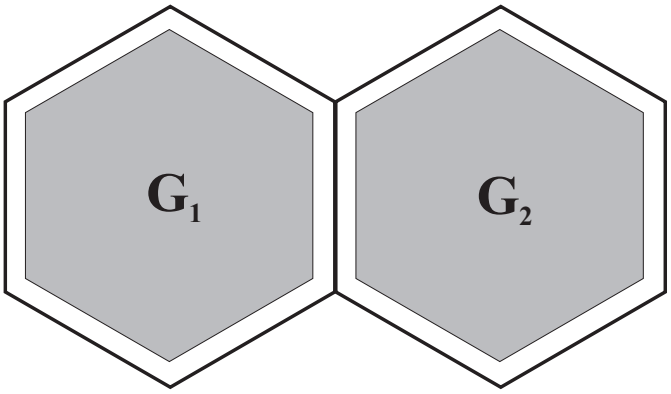

Fig. 1. Piston definition. The integration zones are shown darker.

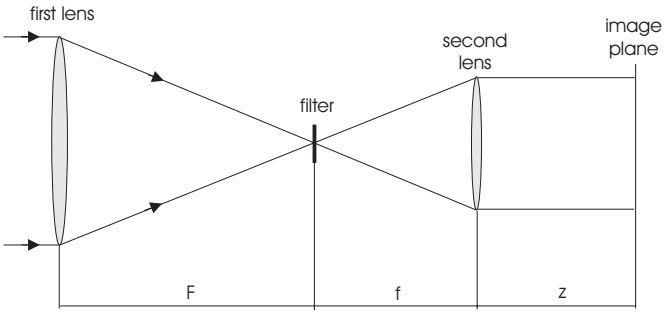

Fig. 2. Fourier plane filtering.

produce large errors in piston reconstruction if the piston is retrieved from near-to-border measurements. For example, to avoid the effects of border defects, the use of opaque masks at a plane conjugated to the intersegment subapertures, covering to some extent the edge of the segment mirrors, has been suggested for the Shack-Hartmann Segment Figure Sensor of GTC (Bello-Figueroa 2000). Hence it is desirable to take certain precautions which would allow one to override the influence of border defects on the piston reconstruction.

Taking into account the above considerations, we can write the averaged piston difference Δ_{12} between the segments 1 and 2 needed for the true co-phasing as

$$\Delta_{12} = \frac{1}{2\pi}\left[\frac{1}{A_1}\int_{G_1} \mathrm{d}^2\rho S(\boldsymbol{\rho}) - \frac{1}{A_2}\int_{G_2} \mathrm{d}^2\rho S(\boldsymbol{\rho})\right], \qquad (1)$$

where the piston is expressed in wavelengths, S is the phase of the initially plane wave reflected by a segmented mirror, G_1 and G_2 denote the integration over the corresponding segments, and A_1 and A_2 are the areas of integration zones. To avoid the border defects, the zones near to the borders are excluded from integration (see Fig. 1).

In this paper we present a new approach allowing us to restore the set of pistons needed for the true co-phasing. This method is based on shearing interferometry (Malacara 1992). Compared to the usual shearing interferometry, however, our method assumes a special choice of the field shift, taking into account the geometry of a segmented mirror. As it will be seen through the paper, this special choice allows one to reconstruct the relative pistons taking into account the segment's aberrations and excluding the effect of border defects. The other advantage of the method is its high sensitivity: even in the presence of high levels measurement noise it allows for very accurate piston reconstruction.

The present paper is the first one that presents the theory of our method and demonstrates its abilities for small pistons reconstruction needed for narrow-band co-phasing. In future publications we are planning to present the development of our method for the broad-band co-phasing, several algorithms of piston reconstruction from turbulence-affected measurements and laboratory test results.

2. Theory of the method

The shearing interferometry can be considered as a part of the Fourier plane filtering approach. This approach was initially suggested by Foucault (1859) and, due to its high sensitivity, turned out to be extremely useful for optical testing. From that time many methods based on the principle of Fourier plane filtering were developed: the wire test (Ritchey 1904), the Zernike test (Zernike 1934) and later shearing interferometry (Ronchi 1964) are just few particular examples of this approach. From the mathematical point of view, this method consists of three main steps: the Fourier transform of the initial field, the filtering of the obtained spatial spectrum (in general, the amplitude-phase filtering), and the Fourier transform of the filtered field. One among the possible experimental setups of this method consists of two lenses and a filter (Fig. 2).

If the separation z is related to the lens focal distances as

$$z = f^2/F + f \approx f, \text{ when } F \gg f,$$

then the field U at the image plane is related to the initial field U_0 at the aperture as

$$U(\boldsymbol{\rho}) = -\left(\frac{k}{2\pi}\right)^2 \frac{\exp[ik(F+2f)]}{Ff}\int_G \mathrm{d}^2\rho_0 U_0(\boldsymbol{\rho}_0) \times \int \mathrm{d}^2\rho_1 g(\boldsymbol{\rho}_1)\exp\left[-ik\boldsymbol{\rho}_1 \times \left(\frac{\boldsymbol{\rho}_0}{F} + \frac{\boldsymbol{\rho}}{f}\right)\right], \qquad (2)$$

where k is the wavenumber, G denotes the integration over the aperture of the first lens, and $g(\boldsymbol{\rho}_1)$ is the filter transmittance function. From the physical point of view the condition $z = f^2/F + f$ means that the output field U is observed at the image plane of the telescope pupil.

Let us consider the filter with a transmittance function

$$g(\boldsymbol{\rho}_1) = \frac{\alpha}{\sqrt{1+\gamma^2}}\left[1 + i\gamma\exp(ibx_1)\right], \qquad (3)$$

where α and γ are the technological parameters related to the filter design $(0 < \alpha \leq 1, 0 < \gamma \leq 1)$.

In the next section we discuss possibility of practical design of this filter. Note that it is not necessary to perform a filter calibration to get the parameters α and γ because, as it will be seen in this section, all the parameters necessary for the piston reconstruction can be obtained directly from the measurements.

Substituting (3) into (2) and performing the integrations we get

$$U(-x,-y) = \frac{m\alpha}{\sqrt{1+\gamma^2}} \times \left[U_0(mx,my) + i\gamma U_0(mx+d,my)\right], \quad (4)$$

where $m = F/f$, and $d = bF/k$.

From the physical point of view, the field U at the image plane is produced by the interference of the direct initial field and the shifted initial field. Representing the field U_0 at the aperture as $U_0(\boldsymbol{\rho}_0) = A\exp\left[iS(\boldsymbol{\rho}_0)\right]$, we can write the intensity I at the image plane as

$$I(-x,-y) = \frac{(m\alpha A)^2}{1+\gamma^2} \times \left\{1+\gamma^2 - 2\gamma\sin\left[S(mx,my) - S(mx+d,my)\right]\right\}, \quad (5)$$

where A and S are the amplitude and the phase of the initial field.

As one can see from (5), the argument of sine is just a differential piston between the aperture points separated by the distance $d = bF/k$. Now let us choose the filter frequency b as

$$b = \frac{ak}{F}, \quad (6)$$

where a is the segment size (see Fig. 4).

The choice (6) of the filter frequency b is the key point of our method. From a physical point of view, this choice provides the proper interference of light coming from the neighboring segments that results in the possibility of restoring the segment-averaged piston difference. Figure 3 illustrates the interference scheme corresponding to the choice (6) of the filter frequency (for simplicity, $F = f$ is assumed in this figure). Geometrically, the image consists of two parts: the map of a segmented mirror plus the map of right-side mirror segments produced by the shifted field. The intensity distribution at the image plane contains the three zones where different physical effects take place.

The interference occurs inside the middle zones of the image plane. As one can see from (5), the intensity at each point of these zones contains the information about the local differential piston (the piston difference between the points $\{x,y\}$ and $\{x+a,y\}$). Using (5) one can express this local differential piston $\Delta(x,y)$ as

$$2\pi\Delta(x,y) = S(mx,my) - S(mx+d,my) = \arcsin\left\{\frac{1+\gamma^2}{2\gamma}\left[1 - \frac{1}{(A\alpha m)^2}I(-x,-y)\right]\right\}. \quad (7)$$

Equation (7) contains the parameters m, A, α, γ related to the filter design, the optical scheme, and the field amplitude at the aperture. However, these parameters are

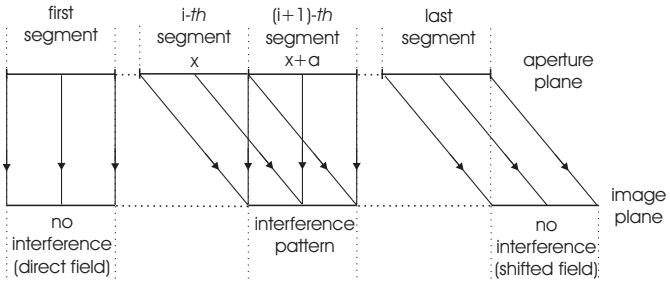

Fig. 3. Interference scheme.

presented in such combinations which can be obtained directly from the measurements in certain image zones. Let us consider the first and the last zone in Fig. 3. The intensities I_d and I_s inside these zones are produced by the direct field and by the shifted field, respectively. As follows from (4), they can be expressed as

$$I_\mathrm{d} = \frac{A^2\alpha^2m^2}{1+\gamma^2}, I_\mathrm{s} = \frac{A^2\alpha^2m^2\gamma^2}{1+\gamma^2}. \quad (8)$$

The terms occurring in (8) are related directly to the certain physical effects which result from the energy conservation law. The intensity of the direct field I_d is a product of the following terms: the irradiance A^2 at the mirror aperture, the overall fraction α^2 of light leaving the filter without absorption, the ratio m^2 of areas of the actual aperture and its image, and the fraction of light $1/\left(1+\gamma^2\right)$ allocated by the filter to the direct image. The intensity of the shifted field I_s differs from the intensity of the direct field I_d only by the factor γ^2 that shows the difference between the fractions of light allocated by the filter to the shifted and direct images, respectively.

Taking into account (8) and integrating the local differential piston $\Delta(x,y)$ over the corresponding image zone one can get the segment-averaged piston Δ between two neighbor segments as

$$\Delta = \frac{1}{2\pi A_\mathrm{i}}\int \mathrm{d}x\mathrm{d}y \arcsin\left\{\frac{1}{2\sqrt{I_\mathrm{d}I_\mathrm{s}}}\left[I_\mathrm{d} + I_\mathrm{s} - I(x,y)\right]\right\} \quad (9)$$

where the integration is performed over the image zone where the related interference occurs, and A_i is the area of the integration zone.

Equation (9) has unique solution in the range $[-\lambda/4, \lambda/4]$ which is the case for the narrow-band co-phasing (Chanan et al. 2000). To get a better accuracy of piston reconstruction, the magnitudes I_d and I_s averaged over the corresponding zones have to be used in (9). The border effect is avoided if the integration zone is chosen in a way that allows one to exclude the border areas from the integration (as is shown in Fig. 1). Taking into account this last consideration and comparing (7) and (9) to (1) one can conclude that the reconstruction procedure above gives the piston defined by Eq. (1). The complete set of piston measurements needed for the co-phasing is obtained if the two channels with different filter orientations

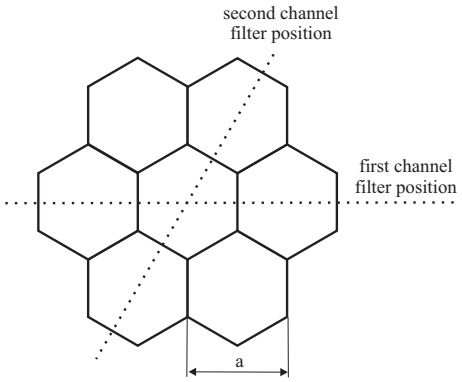

Fig. 4. Filter positioning.

are used. The choice of optimum filter orientation depends on the segmented mirror geometry (for the case of hexagonal segments these orientations are shown in Fig. 4).

The method presented allows us to reconstruct not only the relative pistons but also more high-order aberrations (relative tilt, relative defocus, etc.). As one can see from Eq. (7), the set of measurements consists of the local phase differences between neighbor segments from which the relative aberration coefficients can be obtained by the least-square fitting of a suitable polynomial set to these data. Relative tilt data can be applied for the mirror co-phasing while higher-order aberrations may be useful for active optics purposes.

Equation (9) can be directly applied for segment piston measurement with natural star sources as long as the phase distortions at the telescope pupil are within the range $[-\lambda/4, \lambda/4]$ This is the case of narrow-band co-phasing for space-based telescopes where the atmospheric turbulence is not a matter of concern. Several proposed designs for the Next Generation Space Telescope (NGST) can be compatible with this setup (information about the NGST can be found, among other sites, at `http://ngst.gsfc.nasa.gov/`). For ground-based telescopes, there are two main ways of practical implementation of this method. The best one is to provide the laser illumination from the primary mirror curvature center. This approach is preferable because it allows one to avoid the turbulence effects on the reconstruction quality. However, for certain cases of practical concern this approach can be inapplicable due to technical difficulties. In this case the natural or artificial star illumination can be used and the piston reconstruction has to be performed from turbulence-affected measurements. We are now developing several methods for such a reconstruction which we will discuss in future publications.

3. Filter design

There are several approaches to obtain a filter with an effective transmission function as given in (3). In principle, it is possible to use standard optical microlithographic techniques to generate it as a combination of a variable absorption filter and a pure phase element, both periodic, with a fundamental spatial frequency given by (6) and absorption and phase profiles determined by the modulus and argument, respectively, of (3). However, this procedure involves rather critical fabrication steps and a strict control of the final results since small fabrication errors will give rise to spurious diffraction orders whose fields would be superimposed on the amplitudes in (4) and consequently disturb the interference pattern (Eq. (5)). A more practical approach is to use a holographically-generated double-frequency diffraction grating similar to that described by Wyant for his lateral shear interferometer (Wyant 1973).

This grating can be obtained by recording onto a suitable photosensitive material (e.g. silver halide plates) the interference pattern of two coherent plane waves tilted with respect to each other and, after this first exposure, changing the tilt angle between the waves and performing a second exposure while keeping the film in its initial position. After developing the film in the linear region of the transmittance-exposure curve we get an optical element whose transmission function is

$$g(\boldsymbol{r}) = c_0 + c_1 \cos(b_1 x + \varphi_1) + c_2 \cos(b_2 x) \tag{10}$$

where c_0, c_1 and c_2 are constant factors determined by the relative amplitudes of the interfering waves and the film response to irradiation, and b_1 and b_2 are the spatial frequencies of the interference fringes recorded in the first and second exposures, respectively. The origin of coordinates for $g(\boldsymbol{r})$ has been taken, without loss of generality, at an arbitrary maximum of the $\cos(b_2 x)$ term. The term φ_1 accounts for the relative de-phasing of both fringe patterns at the origin of coordinates. Expanding the cos in exponents and allowing for a lateral displacement δ of such a filter in its own plane we get

$$\begin{aligned} g(\boldsymbol{r}) \;=\; & c_0 + \frac{c_2}{2} \exp(i b_2 \delta) \exp(i b_2 x) \\ & \times \left\{ 1 + \frac{c_1}{c_2} \exp\left[i \left(\varphi_1 + (b_1 - b_2)\, \delta \right) \right] \exp\left[i \left(b_1 - b_2 \right) x \right] \right\} \\ & + c.c., \end{aligned} \tag{11}$$

where *c.c.* stands for the complex conjugate of the second term.

Note that this second term has two subterms inside the brackets (of relative amplitudes 1 and c_1/c_2) which will give rise at the observation plane to two images of the primary mirror laterally shifted by an amount $(b_1 - b_2)\, F/k$ (in coordinates scaled as in the input plane), and with a relative phase shift $\varphi_1 + (b_1 - b_2)\, \delta$. This phase shift can be easily tuned to $\pi/2$ by properly choosing the displacement δ. The second term is multiplied by the factor $\exp(i b_2 x)$ before the brackets, which is essential in this scheme: it gives rise to an overall lateral shift of both interfering images. Choosing b_2 such that $b_2 \geq kR/F$, where R is the radius of the telescope primary mirror, we can separate at the observation plane the two images of the mirror produced by the second term from those produced

by the first term (c_0) which remain centered at the origin, and those due to the third term, the complex conjugate of the second, which suffer an overall lateral shift in the opposite direction. In this way we avoid the multiple-beam overlapping and we get in a definite region of the output plane just the interference pattern due to an equivalent filter

$$\frac{c_2}{2}\left[1 + i\frac{c_1}{c_2}\exp\left[i\left(b_1 - b_2\right)x\right]\right] \tag{12}$$

which is the same as that in (3), with parameters $b_1 - b_2 \equiv b$, $c_2/2 \equiv \alpha/\sqrt{1+\gamma^2}$ and $c_1/c_2 \equiv \gamma$. The only difference is that due to the $\exp(ib_2x)$ factor this interference pattern is not centered at the origin of coordinates of the observation plane, but this is not troublesome.

The lateral shifts along two different angular orientations necessary to scan completely the segmented primary mirror can be obtained using two independent observation channels with filters rotated by 60° with respect to each other or using a single channel with a modified filter combining both functions. To manufacture that filter we proceed as before but after the first two exposures have been made, the film is rotated in its own plane by 60° and two identical exposures are performed. A two-dimensional grating is thus formed, giving rise at the observation plane to several images laterally shifted along the desired directions. This filter differs from Wyant's one (Wyant 1973) only in its design parameters. Wyant's grating was developed for a lateral shear interferometer intended to measure the wavefront slopes by finite phase differences, so that the relative displacement between the interfering images was very small, while in our application this relative shift has to be big enough to allow superimposing of two adjacent segment images. On the other hand, in Wyant's grating the diffracting structures were oriented at 90° from each other, in order to measure the orthogonal components of the wavefront slopes, while here the angle between these structures is determined by the hexagonal lattice of the segmented mirror.

This double frequency filter has to be carefully positioned at the mirror focal plane, since the relative phase between interfering images (which we set to $\pi/2$) is very sensitive to δ. The requirement is that δ has to be kept constant to a small fraction of $L = 2\pi/\left(b_1 - b_2\right)$. Taking as typical figures those of Keck at visible wavelengths ($F = 150$ m, $R = 5$ m, $a = 1$ m, $\lambda = 0.5$ μm), we have $L = 75$ μm.

The crucial factors to get a good quality filter are not different from those standard in holography: starting from good optical quality plane waves, keeping the holographic setup well aligned and stable during the double-exposure process and using a suitable photosensitive recording medium. The spatial bandwidth requirements of the recording medium are fairly moderate: in order to avoid undesired overlapping at the observation plane we need to record interference fringes with a spatial period equal to or smaller than $\Lambda = 2\pi/b_2 = \lambda F/R$.

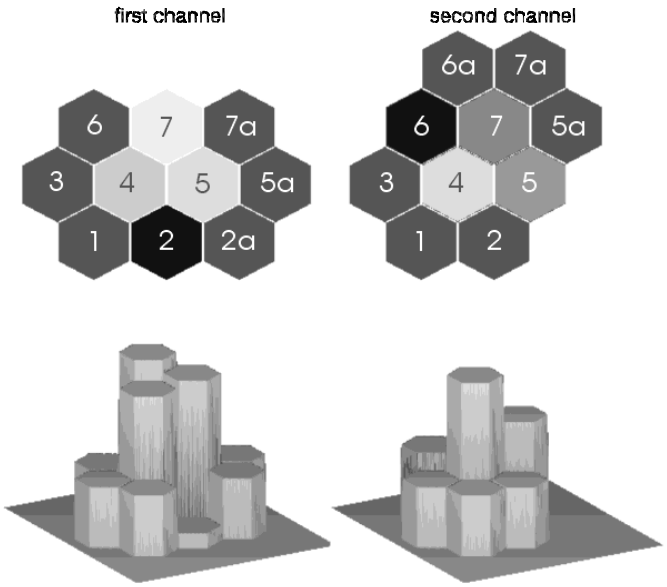

Fig. 5. Intensity at the image plane (noiseless case). First channel. The interference occurs inside the zones 2, 4, 5, 7. The relative pistons Δ_{ij} between ith and jth segments are reconstructed from the following zones: Δ_{12} – zone 2, Δ_{34} – zone 4, Δ_{45} – zone 5, Δ_{67} – zone 7. The parameter $I_{\rm d}$ can be obtained from the zones 1, 3, 6, while parameter $I_{\rm s}$ can be obtained from the zones 2a, 5a, 7a. Second channel. The interference occurs inside the zones 4, 5, 6, 7. The relative pistons are reconstructed from the following zones: Δ_{14} – zone 4, Δ_{25} – zone 5, Δ_{36} - zone 6, Δ_{47} – zone 7. The parameter $I_{\rm d}$ can be obtained from the zones 1, 2, 3, while the parameter $I_{\rm s}$ can be obtained from the zones 5a, 6a, 7a.

Using the above parameters for a typical 10 m-class segmented telescope this would mean $\Lambda = 15$ μm, i.e. recording about 67 fringes per mm, which is well with the present capabilities.

4. Simulation results

We perform a simulation for the case of hexagonal segments shown in Fig. 4. It is assumed that the image of a single segment contains about 80 000 pixels that correspond to the Keck-like telescope (36-segment mirror, 2048×2048 pixels CCD). Two cases are included into the simulation: the noiseless case (just to stress the salient features of the observed image) and the more realistic one when the signal at each pixel of the image $I(x, y)$ is corrupted by noise arising from several sources (photon noise, CCD readout, etc.). Noisy data have been simulated adding random gaussian noise with zero mean and standard deviation equal to 30% of $I(x, y)$ to the irradiance $I(x, y)$ at the image plane.

The corresponding pictures are shown in Figs. 5 and 6, while the numerical results are presented in Table 1. The initial magnitudes of relative pistons are chosen randomly with respect to the central segment, then they are reconstructed from the set of measurements obtained from two

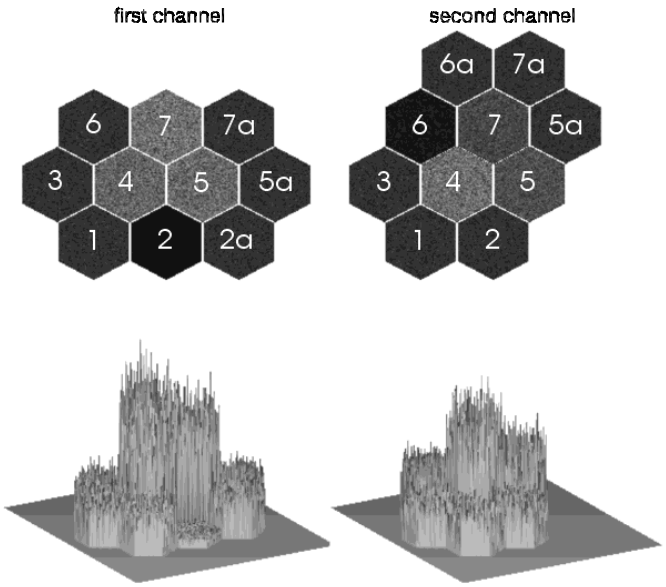

Fig. 6. Intensity at the image plane (30% of noise).

Table 1. Simulation results.

piston number	initial piston	reconstructed piston (no noise)	reconstructed piston (30% noise)
Δ_{41}	$-\lambda/8.0$	$-\lambda/8.0$	$-\lambda/8.0$
Δ_{42}	$\lambda/21.0$	$\lambda/21.0$	$\lambda/21.0$
Δ_{43}	$\lambda/35.0$	$\lambda/35.0$	$\lambda/34.8$
Δ_{45}	$-\lambda/26.0$	$-\lambda/26.0$	$-\lambda/26.1$
Δ_{46}	$\lambda/30.0$	$\lambda/30.0$	$\lambda/29.9$
Δ_{47}	$-\lambda/45.0$	$-\lambda/45.0$	$-\lambda/45.4$

channels. The reconstruction details are outlined in the caption of Fig. 5.

As one can see from Table 1, the method allows a high-accuracy piston reconstruction even in the presence of the significant measurement noise. It takes place because the noise effect cancels efficiently by the segment averaging procedure.

5. Conclusions

A new method of piston measurements based on the shearing interferometry has been developed. It has been shown that the method combines a high accuracy of piston reconstruction with the ability to restore the pistons, taking into account a segment's aberrations. The simulation results have shown that the method works quite well even in the presence of strong measurement noise.

Acknowledgements. The authors are grateful to Dr. J. M. Beckers for helpful comments which allowed us to improve the manuscript.

This work was supported by the Conasyt project 34517-E (Mexico) and by the DGAPA-PAPIIT project IN115399 (Mexico).

References

Bello-Figueroa, C. D. 2000, Ph.D. Thesis, IAC – Univ. de La Laguna, 144, 169
Chanan, G., Troy, M., Frank, D., et al. 1988, Appl. Opt., 37, 140
Chanan, G., Troy, M., & Sirko, E. 1999, Appl. Opt. 38, 704
Chanan, G., Troy, M., & Ohara, K. 2000, Proc. SPIE, 4003, 188
Cuevas, S., Orlov, V. G., Garfias, F., Voitsekhovich, V. V., & Sanchez, L. 2000, Proc. SPIE, 4003, 291
Foucault, L. M. 1859, Ann. Obs. Imp. Paris, 5, 197
Malacara, D. 1992, Optical Shop Testing, ed. D. Malacara (John Wiley & Sons, New York)
Orlov, V. G., Cuevas, S., Garfias, F., Voitsekhovich, V. V., & Sanchez, L. 2000, Proc. SPIE, 4004, 540
Ritchey, G. W. 1904, Smithson. Contrib. Knowl. 34, 3
Rodriguez-Ramos, J., & Fuensalida, J. 1997, Proc. SPIE, 2871, 613
Rodriguez-Ramos, J., & Fuensalida, J. 2000, Proc. SPIE, 4003, 270
Ronchi, V. 1964, Appl. Opt., 3, 437
Wyant, J. C. 1973, Appl. Opt. 12, 2057
Zernike, F. 1934, MNRAS, 94, 371